**Thesis Project Portfolio**


**Design of a Light Attack Aircraft for the AIAA Undergraduate  Competition**
(Technical Report)


**Military Funding of 5G Technology and the Spin Around  Concept**

(STS Research Paper)



An Undergraduate Thesis

Presented to the Faculty of the School of Engineering and Applied Science
University of Virginia • Charlottesville, Virginia

In Fulfillment of the Requirements for the Degree
Bachelor of Science, School of Engineering



**Brendan Kroger Schneider**
Spring, 2020
Department of Aerospace Engineering

# AIAA 2020-2021 Undergraduate Capstone Project
# Austere Field Light Attack Aircraft
## "The WB-26"

### Final Design Report

Presented by: Team Wade Boggs

University of Virginia

Department of Mechanical and Aerospace Engineering

May 7, 2021

**Team Members**
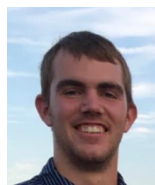
Will Ayscue
AIAA Member 1241680
Team Leader and Mission Analysis Lead

David Gibbs
AIAA Member 1241677
Survivability and Models Lead

Catherine Hanafin
AIAA Member 1179740
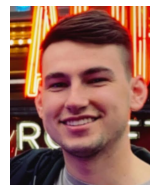Propulsion Lead

Lauren Hancock
AIAA Member 1180477
Aerodynamics Lead

Blake Mager
AIAA Member 1192854
Structures and Weights Lead

Brendan Schneider
AIAA Member 1180759
Cost Analysis Lead

Hope Wheeler
AIAA Member 1180094
Certification Lead

Dr. Jesse R. Quinlan
AIAA Member 306245
Faculty Advisor

# Contents

# Acknowledgements

## Abbreviations

AAA - Advanced Aircraft Analysis

AIAA - American Institute of Aeronautics and Astronautics

AR - Aspect Ratio

CG - Center of Gravity

JSSG - Joint Service Specification Guide

LAA - Light Attack Aircraft

MIL-STD - Military Standard

RFP - Request For Proposal

TOGW - Takeoff Gross Weight

## Executive Summary

This proposal covers the preliminary design and sizing of the WB-26 Light Attack

Aircraft designed by Team Wade Boggs from the University of Virginia. The design is equipped

with twin PT6A-65 engines. As seen in Figure 1, the wingspan is 36 feet and the fuselage length

is also 36 feet. Performance characteristics are seen in Table 1. The total acquisition cost is

expected to be $2.367B for 250 aircraft, and the total operating cost is expected to be $15.258B.

The cost per aircraft is estimated at $10.614M.  The WB-26 is capable of satisfying all of the

RFP requirements, which are laid out in Table 2.
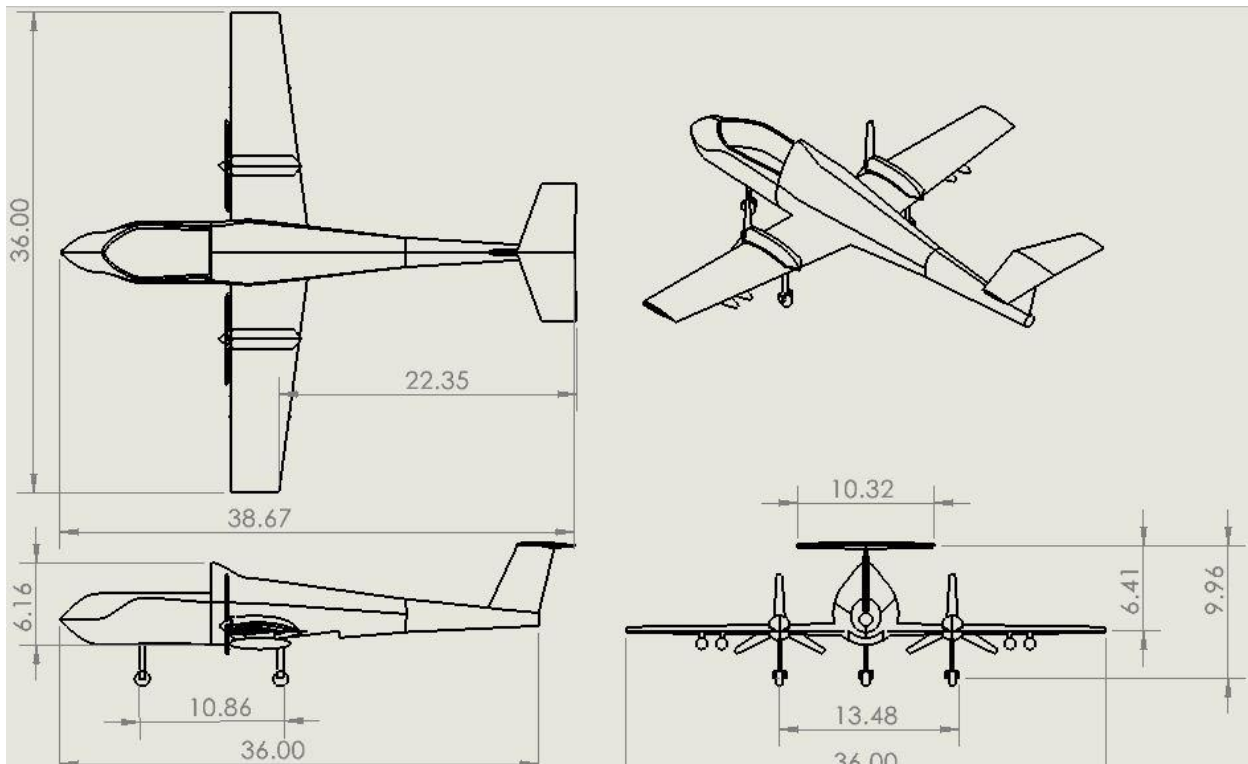


Figure 1: Dimensioned drawings of the final design

Table 1: Summary of Performance Characteristics

| | |
|---|---|
| TOGW | 16,334 lb |
| Block Fuel Burn | 5,398 lb |
| TSFC | 0.1778 lb/(lb*h) |
| CG Location | 16.4 ft from nose |
| Wing Area | 172.8 ft$^2$ |
| $C_L$ cruise | 0.5 |
| $C_L$ max | 2.55 w/ flaps |
| AR | 7.5 |
| $C_{D.tot}$ cruise | 0.032 |
| $C_{D,tot}$ takeoff/landing | 0.2 |
| Takeoff Length | 3,215 ft |
| Landing Length | 3,309 ft |

# 1. Requirements Analysis

This section will discuss the requirements of the AIAA RFP for an austere field light attack aircraft and the subsequent constraints put on the design process.

## 1.1 Requirements & Objectives

The AIAA RFP contains requirements, objectives, and additional constraints for the design of the austere field light attack aircraft proposals. Table 2 reviews the requirements and objectives from the RFP.

Table 2: Requirements and objectives for the 2021 AIAA design challenge (AIAA, 2020).

| Category | Area of Design | Description |
|---|---|---|
| Required | Austere Field Performance | Takeoff and land over a 50 ft obstacle in shorter than 4,000 ft when operating from austere fields at a density altitude up to 6,000 ft with semi- prepared runways, such as grass or dirt surfaces with California Bearing Ratio of 5 |
| Required | Payload | 3000 lbs of armament (minimum) |
| Required | Armament Types | Integrated gun for ground targets |
| Required | Service life | 15,000 hours over 25 years |
| Required | Service ceiling | Greater than 30,000 ft |
| Required | Crew | Two, both with zero-zero ejection seats |
| Objective | Survivability | Consider armor for the cockpit and engine, reduced infrared and visual signatures, and countermeasures (chaff, flares, etc.). |
| Objective | Armament Types | Provisions for carrying/ deploying a variety of weapons, including rail-launched missiles, rockets, 500 lb (max) bombs |
| Derived Objective | Affordability | Provide a "best value" design that meets mission specifications outlined in section 1.3 with consideration for both acquisition and operational cost over the expected 25-year service life |

The California Bearing Ratio of 5 indicates that the aircraft needs to be capable of taking off from semi-prepared runways. It will also be crucial to satisfy the three objectives to make our design the best solution for this challenge.

The RFP additionally requires the LAA to be more survivable than helicopters currently used for these types of missions.We believe our project deliverable will open up a sect of operating terrains that have historically been off limits for aircraft. As helicopters are typically used in these quick, tactical, battle situations but they do not have the protection nor can they carry the amount of armament that a light attack aircraft has, we hope to offer an aircraft that will provide air support for fighting troops in places like short grass fields, and rocky or clay ground.

The design also needs to be certifiable for military standard airworthiness and follow JSSG protocols. Designing with the future in mind, our proposal has design aspects that are adaptable to fit with the next generation of military missions.

## 1.2 Reference LAA

After assessing the requirements and objectives put forth for the AIAA challenge, our team utilized the performance characteristics and design sizing of other light attack aircraft on the market to inspire the direction of our design. Currently, the United States Army and Air Force employ two LAA: A-29 Super Tucano and A-T6 Wolverine (AOPA, 2020). They are both low mass but carry a different assortment of armaments to distinguish themselves from each other. Although these aircraft have proven to be successful in their respective missions, there is one limiting design aspect that keeps them from being successful in all types of battle situations. This is the fact that they are not designed to operate from austere fields. An austere field is terrain that lacks ramp space or navigation aids, or has a poor ground surface such as flexible pavement, grass, or dirt. The A-29 and the A-T6 can only fly missions where there is a properly functioning airstrip nearby.

Both aircraft have a single turboprop engine with seats for two crew members. The A-29 has a service ceiling of 35,000 feet, a maximum range of 2,600 nautical miles, a loiter time of roughly six and a half hours, and a landing distance of around 2,800 feet (Sierra, 2018). The A-T6 has a service ceiling of 31,000 feet, a maximum range of 1,725 nautical miles, and a loiter time of roughly seven and half hours (AOPA, 2020). The performance characteristics of these aircraft are stable comparators for the mission requirements in the AIAA RFP.

## 1.3 Mission Profile

There are two mission profiles as outlined in the RFP. The first, the Design Mission, stipulates that the aircraft carry the full payload of 3,000 lb of armaments to station, and then loiter on station for four hours. The second, the Ferry Mission, requires only 60% of the Design Mission's payload, but must cover a range of 900 n.m.

The two mission profiles are graphically represented below in Figures 2 and 3, and both include the reserve portion at the end of the missions.
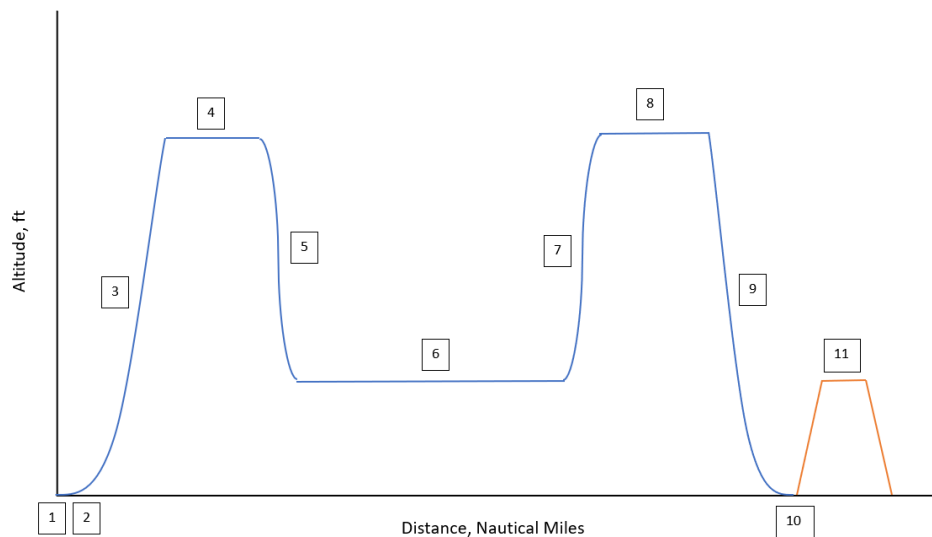


Figure 2: Design Mission Profile. Each point corresponds to the following aspect of the mission: 1: Warm Up / Taxi, 2: Take Off, 3: Climb, 4: Cruise, 5: Descent, 6: Loiter, 7: Climb, 8: Cruise, 9: Descent / Landing, 10: Taxi / Shutdown, 11: Reserves
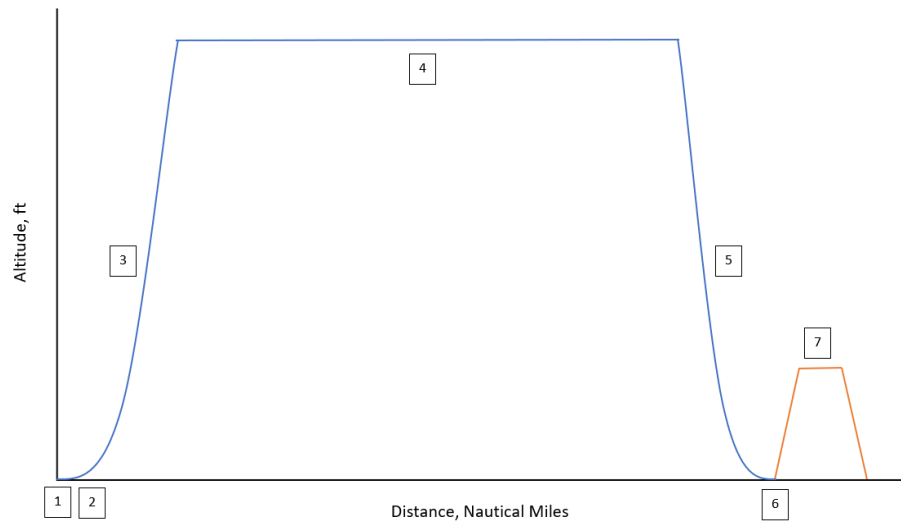
Figure 3: Ferry Mission Profile. Each point corresponds to the following aspect of the mission: 1: Warm Up/Taxi, 2: Take Off, 3: Climb, 4: Cruise, 5: Descent/Landing, 6: Taxi/Shutdown, 7: Reserves

## 1.4 Key Design Drivers & Technologies

One of the focusses of the RFP is to ensure that the LAA can safely take off and land on short, unfinished airfields. This dictated the majority of our trade studies as we attempted to maximize lift at takeoff, and L/D during approach and landing. In addition, this guided our design towards being as lightweight as possible in order to achieve the short field takeoff and landing. Robust landing gear and foreign object considerations are also necessary because of the unfinished airfield capability outlined by the RFP. Another main consideration in the design process was cost. Using off-the-shelf components and minimizing weight and complexity, while keeping service costs down was also a consideration.

## 1.5 Airworthiness Certification Requirements

Design for certifiability is the term used to describe the process of ensuring that any technology or artifact is compliant with laws and specifications put in place that pertain to the

said item. The process of certifying is necessary because there is no moving forward in the manufacturing of the aircraft if the work and resources put into developing the design leads to no certification. The standards and specifications which control the design certifications of a military grade aircraft are found in Military Standards and Joint Service Specification Guides. Combining the RFP requirements with the MIL-STD and JSSG constraints provide a complete set of rules that govern the design of our proposal. In addition to ensuring that the MIL-STDs and JSSGs are followed, it is also important that our design process is mapped to the Technology Readiness Level (TRL) model.

### 1.5.1 MILSTD /JSSG Requirements

The MIL-STDs and JSSGs that specifically address the design certifications of an aircraft are found in the Airworthiness Certification Criteria Handbook, or MIL-HDBK-516, JSSG-2001 Air Vehicle, JSSG- 2006 Aircraft Structures, JSSG -2007 Engines, Aircraft, Turbine, JSSG -2009 Air Vehicle Subsystems, and JSSG -2010-7 Crash Protection Hand. The group specifically targeted sections of these standards that we believed were the most crucial and limiting to the design. These areas included: structures, flight technology and vehicle performance, propulsion system, air vehicle subsystems such as survivability, crew systems,and armaments and stores integration. Detailed tabs were placed on specific regulations within these areas for quick and easy reference, such as Table 3.

Table 3: Crew Systems

| Section number | Area of interest | Reference |
|---|---|---|
| MIL-STD-516C, 9.1.1 | Escape systems: safety compatibility, escape reliability | Page 357-359 of MIL-HDBK-516C JSSG-2010 Crew Systems |
| MIL-STD-516C, 9.2.1.2 | Interior and exterior fields of view | Page 363-364 of MIL-HDBK-516C |
| MIL-STD-516C, 9.2.5 | Emergency controls: ejection seating | Page 366 of MIL-HDBK-516C |
| MIL-STD-516C, 9.4.4 | Crew system interface: cabin sizing | Page 375 of MIL-HDBK-516C |
| MIL-STD-516C, 9.6.1 and 9.6.5 | Transparency integration and optical characteristics for canopy and ejection seats | Page 380, 382 of MIL-HDBK-516C JSSG-2010-14 |
| MIL-STD-516C, 9.7.1 | Ejection seating system load capabilities | Page 384 of MIL-HDBK-516C |

**1.5.2 Technology Readiness Level**

The RFP requires our design to have critical technologies on our aircraft at TRL 8 or higher by their entry into service in 2025. TRL 8 is reached when a technology is proven to work in its final form and operational conditions. Some technologies on the aircraft that we believe to be critical here are the engines, which are discussed in section 4.3, and the landing gear, discussed in section 8.1.

## 2. Design Process

### 2.1 Concept Downselect

In order to move forward with a design for a light attack aircraft, many design options were researched and considered. Each design option was reviewed by the entire team and given ratings based on how they optimized different design aspects. This process helped ensure an unbiased method of designing that can meet the specific requirements laid out in the RFP. The downselect methodology can be seen in Table 4. This methodology follows the interactive reconfigurable matrix of alternatives (IRMA). In a detailed research paper done by the Georgia Institute of Technology explaining the benefits of this concept selection process, "IRMA aids designers by bringing tacit knowledge and zeroth order metrics into a collaborative design tool. It ensures that interrelationships between concept options are captured and displayed." (Engler, Biltgen, and Mavris, 2007).

Based on the detailed analysis and benefits that this type of methodology provides, our team moved forward with analyzing each alternative against a metric based on merit. Each of the design alternatives listed in the first column were compared based on the different metrics listed in the first row and were ranked on a scale from -5 to 5; -5 being detrimental, 0 being neutral, and 5 being beneficial. The selected components can be seen highlighted in green, and almost all of them ended up being incorporated into the final design with the exception of the wing shape. It was instead decided to move forward with a tapered wing to reduce weight and drag, which will be further discussed in later sections.

Table 4: Concept downselect of different design components

| Alternatives | Stealth | Survivability | Fuel Efficiency | Weight | Maneuveribility | Quick Takeoff/Landing | Service Height | Cost | | Totals |
|---|---|---|---|---|---|---|---|---|---|---|
| **Number of Engines** | | | | | | | | | | |
| 1 | -1 | -3 | 0 | -1 | 0 | 0 | 0 | 0 | | -5 |
| 2 | -3 | 2 | -3 | -3 | 3 | 3 | 2 | -3 | | -2 |
| **Propulsion System** | | | | | | | | | | |
| turboprop | -2 | 0 | 4 | 2 | 0 | 1 | 2 | 0 | | 7 |
| turbofan | 0 | 0 | -2 | -2 | 1 | 3 | 3 | -5 | | -2 |
| **Pitch of Blades** | | | | | | | | | | |
| variable | 0 | -1 | 2 | -1 | 2 | 4 | 0 | -1 | | 5 |
| fixed | 0 | 0 | 0 | 0 | 0 | 0 | 0 | 0 | | 0 |
| **Number of Blades** | | | | | | | | | | |
| 3 | 0 | 0 | 0 | 0 | 0 | 0 | 0 | 0 | | 0 |
| 4 | -1 | 0 | 0 | -1 | 1 | 1 | 0 | -1 | | -1 |
| 5 | -2 | 0 | 0 | -2 | 2 | 2 | 0 | -2 | | -2 |
| **High Lift System** | | | | | | | | | | |
| flaps | 0 | 2 | 0 | 0 | 0 | 2 | 0 | -1 | | 3 |
| STOL/VTOL | 0 | -1 | -1 | -3 | 2 | 5 | 0 | -3 | | -1 |
| **Wing Shape** | | | | | | | | | | |
| rectangular | 0 | 0 | 3 | 0 | 0 | 0 | 0 | 0 | | 3 |
| small taper | 0 | 0 | 0 | 1 | 1 | 0 | 0 | -1 | | 1 |
| high taper | 0 | 0 | 0 | 2 | 2 | 0 | 0 | -2 | | 2 |
| box wing (biplane) | -4 | -4 | -1 | -3 | -5 | -2 | 0 | -3 | | -22 |
| **Wing position** | | | | | | | | | | |
| top of fuselage | 0 | 0 | 0 | 0 | -5 | -3 | 0 | 0 | | -8 |
| bottom of fuselage | 0 | 0 | 0 | 0 | 3 | 3 | 0 | 0 | | 6 |
| middle of fuselage | 0 | 0 | 0 | 0 | 0 | 1 | 0 | 0 | | 1 |
| **Wing sweep** | | | | | | | | | | |
| 0-5 | 0 | 0 | 0 | 0 | 0 | 0 | 0 | 3 | | 3 |
| 5-10 | 0 | 0 | 1 | -1 | 1 | -1 | 0 | -1 | | -1 |
| 10 or higher | 0 | 0 | 2 | -2 | 2 | -2 | 0 | -2 | | -2 |
| **Tail Configuration** | | | | | | | | | | |
| T-tail | 0 | 0 | -1 | -1 | 1 | 2 | 0 | -1 | | 0 |
| V-tail | 0 | 0 | 0 | 0 | 0 | 0 | 0 | 0 | | 0 |
| **Number of hardpoints** | | | | | | | | | | |
| 3 | 0 | 0 | 0 | 0 | 0 | 0 | 0 | -1 | | -1 |
| 4 | 0 | 0 | 0 | -1 | 0 | 0 | 0 | -2 | | -3 |
| 5 | 0 | 0 | 0 | -1 | 0 | 0 | 0 | -3 | | -4 |
| 6 | 0 | 0 | 0 | -1 | 0 | 0 | 0 | -4 | | -5 |
| **landing gear config** | | | | | | | | | | |
| 1 in front, 2 in back | 0 | 0 | 0 | 0 | 0 | 2 | 0 | -1 | | 1 |
| 2 in front, 1 in back | 0 | 0 | 0 | 0 | 0 | 0 | 0 | 0 | | 0 |

## 2.2 Design Processes and Sizing

To start the initial design process an estimation of the takeoff gross weight was calculated to start sizing aircraft components. The methods used to estimate the initial TOGW were derived from Nicolai and Carichner (2000). This estimation is based on empirical methods based on historical data from previous aircraft. To do this, first the fuel fraction coefficients were calculated for both the design and ferry missions (Appendix A). After the fuel fraction coefficients were calculated, the TOGW was estimated using the aforementioned methods, resulting in an initial weight estimation of 15,049 lbs (Appendix A).

## 2.3 Final Concept Summary

Figure 4, seen below, depicts the final design that our team decided on. The WB-26 features two turboprop engines mounted on the wings. The design features a T-Tail as well as non-swept, tapered wings. Single slotted flaps span 60% of the wing to provide high lift. The tricycle landing gear consists of one nose, and two wing-attached wheels. An integrated machine gun in the nose of the plane compliments the external payloads, as well as the internal bomb bay capable of housing 500 lb Mk-82 bombs. The cockpit features military standard visibility for the pilots, as well as two zero-zero ejection seats.
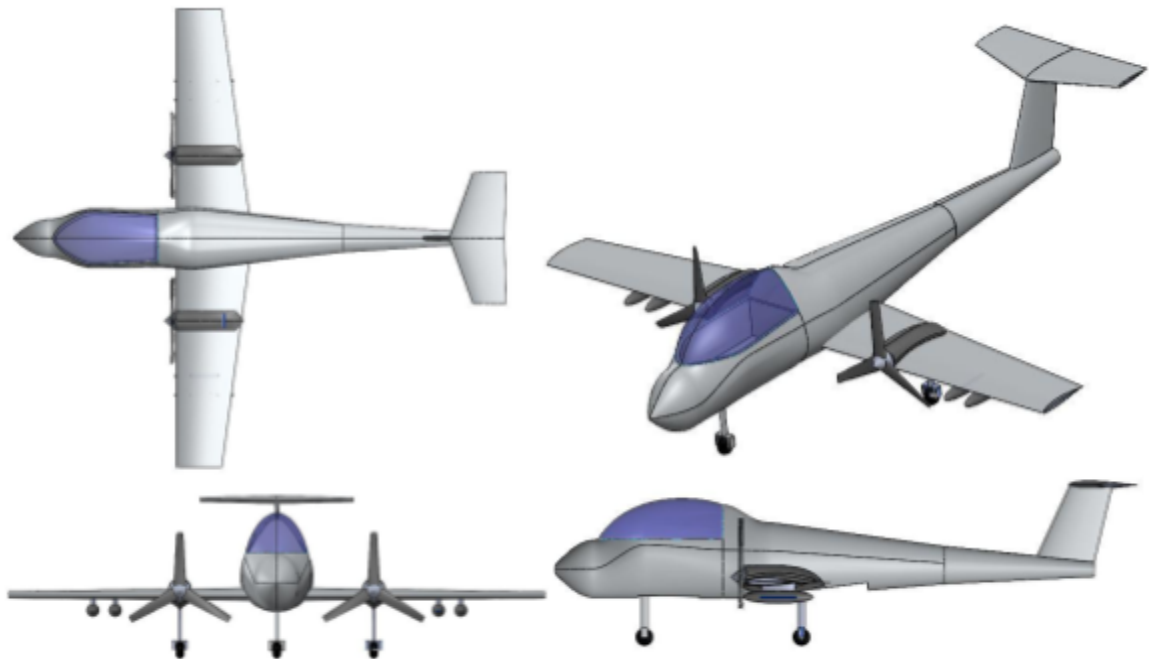


Figure 4: Final Concept

## 2.4 Fuselage

The fuselage is 36 feet in length with a maximum height of 6.26 feet and a maximum depth of 5 feet. This allowed for enough volume to construct all of the necessary internal components. Starting from nose to tail, our nose houses all majority of the avionics sensors including but not limited to the air data computer, radar altimeter, gyrocompass, terrain-following radar and gun camera. Additionally, in the nose there are two FN M3P 50 caliber machine guns responsible for providing close air support. Next, the cockpit houses two pilots seated in ACES ii ejection seats. These need a total of 10 feet of lateral housing distance and five feet of vertical room. Underneath the cockpit is the internal compartment which stores the nose landing gear. Moving backwards the internal bomb bay can house two mk 82 bombs side by side, each weighing 500 lbs. Additionally, above the internal bomb bay is fuel storage to complement the wings with a total capacity of 500 lbs. Lastly, behind the internal bomb bay is where the chaff and flares are held for countermeasure purposes. Figure 5 shows a dimensioned schematic of the fuselage.
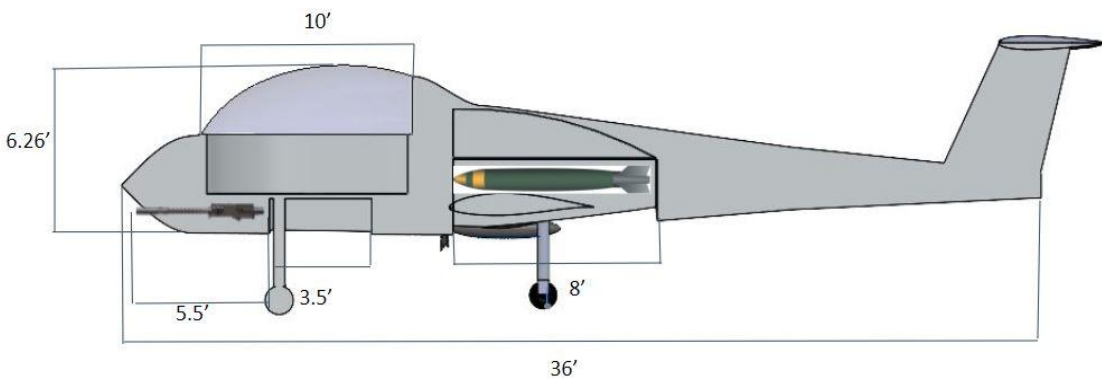


Figure 5: Fuselage cutaway image of internal components

**2.5 Tail**

After conducting a trade study between a V-tail configuration and a T-tail configuration, the T-tail was chosen due to its superior performance at low airspeeds. This is a vital characteristic for the LAA since it will be taking off from Austere airfields with limited runway space, so getting off the ground as soon as possible is essential. The tail volume coefficient approach was used to size both the vertical and horizontal stabilizer as seen in equations 1 and 2. The horizontal stabilizer was bound to the following parameters: wingspan of 10.3 feet, cord of 3.4 feet, AR of 2.9, sweep of 20°, and a taper ratio of 0.6. Additionally, a NACA 0009 airfoil was chosen based on historical data stemming from similar aircrafts with a t-tail configuration. Sizing the vertical stabilizer was more thought provoking based on the trade study conducted. T-tail configurations are at risk for encountering the spoiled air at high AOAs from the main wing, so choosing the correct height was iterative. After calculating the tail volume coefficient the height was varied and ran through VSPaero to make sure the stream lines were not coming into contact with the horizontal stabilizer until an AOA of 16°. The height of the vertical stabilizer was then evaluated to be 5.2 feet above the fuselage. Other characteristics include: root cord of 4 feet, AR of 1.6, sweep of 25°, and taper of 0.7. A NACA 0010 was chosen over the NACA 0009 since it is thicker and that would help with structural purposes. A visual of the tail is seen in Figure 6.

$$C_{VT} = \frac{\ell_{VT}\, S_{VT}}{b\, S_{ref}}$$

Eq.[1]

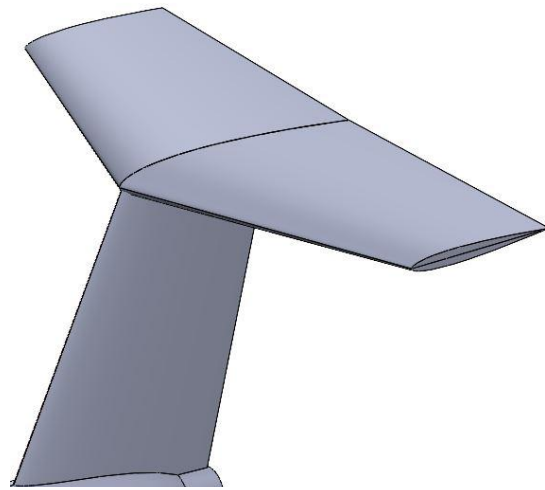$$C_{HT} = \frac{\ell_{HT}\, S_{HT}}{\bar{c}\, S_{ref}}$$

Eq.[2]

Figure 6: Isometric view of tail configuration

## 3. Aerodynamics

Typically for an aircraft, the goal is to achieve maximum lift with minimum drag. For a light attack aircraft, reduced weight also becomes a priority. When considering these three important aspects, it is impossible to completely optimize each one. Therefore, many compromises have to be made when designing a wing, where each design component might improve one aspect while being detrimental to the other.

### 3.1 Airfoil Design

In order to achieve maximum lift with little drag for a light attack aircraft, research into airfoil performance and other similar aircraft designs were taken into consideration. When designing the airfoil, it was decided that it would be beneficial to choose two different airfoils for the root of the wing and the tip of the wing. The airfoil at the root would have a higher camber to increase lift, and slowly decrease in camber to the other airfoil at the tip. This allows for high lift while decreasing weight and drag towards the tip, and provides a more optimal lift distribution across the wing. Furthermore, this allows the ability to select a slightly more supercritical airfoil

for the tip which moves the transition point from laminar to turbulent flow closer to the leading

edge, keeping the boundary layer attached longer. A lot of NACA airfoil data that is available to

the public was examined after an approximate Reynolds number (shown in Equation 3) was

calculated based on the service ceiling outlined in the RFP, and the estimated cruise velocity and

aspect ratio of other similar LAAR. This calculation showed a better approximation for the lift

and drag coefficients at various angles of attack, the plots of which are available to the public

through airfoiltools.com.

$$Re \ = \ \frac{\rho * V * L}{\mu}$$
<div align="right">Eq. [3]</div>

More specifically, the data and plots of the airfoils of the AT-6 Wolverine and the A-29

Super Tucano were closely studied since they are similar light attack aircraft designs, which led

to the final 2 airfoil design choices. One of the options was a NACA 2215 at the root with a

NACA 2412 at the tip, and the other option was a NACA 63-415 at the root and a NACA 63-412

at the tip. The exact measurements of these different airfoils were extracted and drawn on

Solidworks, resulting in 3-dimensional models of both wing options. A CFD analysis was run

through Solidworks, which showed a higher lift-to-drag ratio for the NACA 63 series. Therefore,

the final airfoil selection for this aircraft was a NACA 63-415 root with a NACA 63-412 tip. The

cross-sectional views of these airfoils along with their lift coefficient characteristics are shown in

Figures 7 and 8.
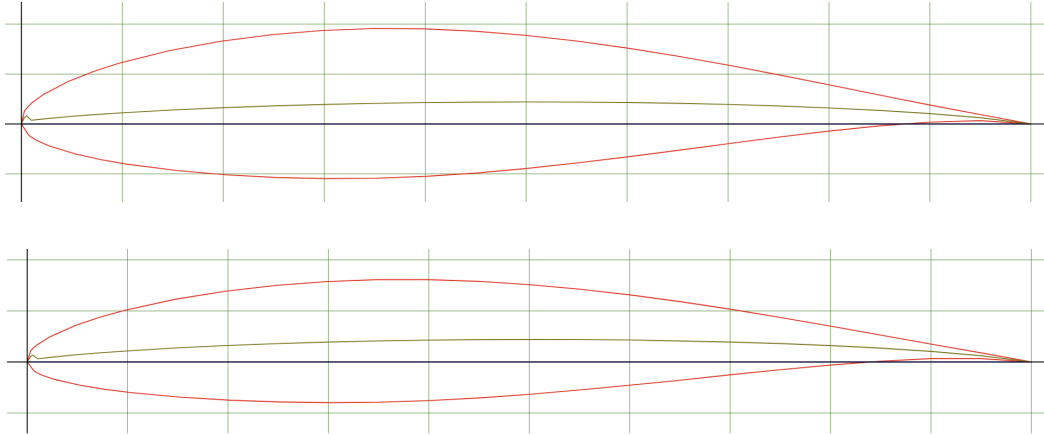
Figure 7: Cross-sectional view of root NACA 63-415 (top) and tip NACA 63-412 (bottom)
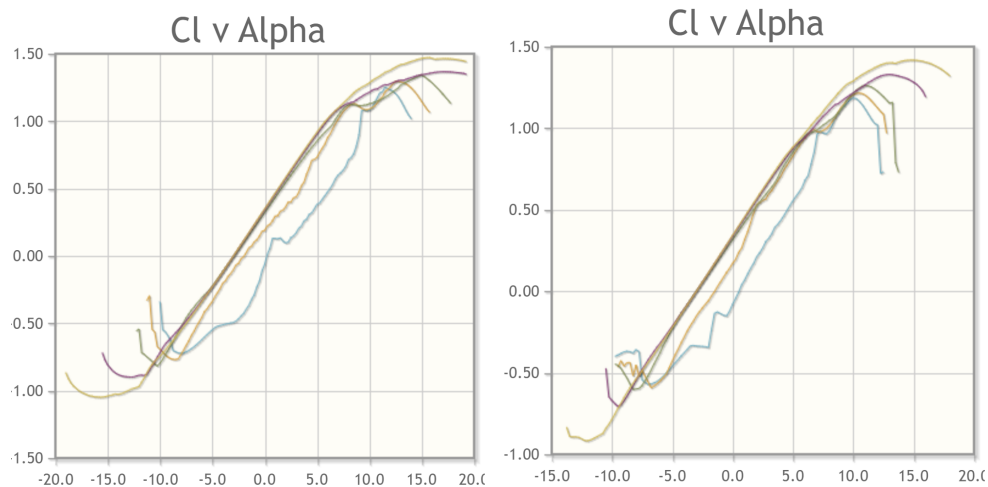


Figure 8: Lift coefficient vs. angle of attack of NACA 63-415 (left) and NACA 63-412 (right)
(based on Re calculation, the purple line in each graph is the one being considered)

## 3.2 Wing Planform

The total wingspan of this aircraft was chosen to be 36 ft due to similarities to other LAA and in order to have enough area to store fuel and house missiles while still being small to keep the weight low. The root chord was originally designed to be 5.625 ft, for the same aforementioned reasons. However, further along in the design process it was discovered that the

chord was too small to hold enough fuel and to house the appropriate armament. Therefore, the

root chord was increased to 6 ft, and a taper ratio of 0.5 was added in an effort to reduce drag and

weight which created an average chord length of 4.8 ft across the span of the wing and an aspect

ratio of 7.5. The original design of the wing surface included winglets to counter wingtip

vortices. However, after running a CFD solver, it was discovered that the winglets added more

drag than they were able to reduce since the wing span is not large enough to add significant

downwash to generate large wingtip vortices. Therefore, the winglets were removed from the

design. Lastly, due to the requirements and priorities of this design, there was no wing sweep

incorporated. A swept wing is typically only beneficial for high speed, supersonic aircraft

because of the decreased surface area that acts against the generated shock waves. At lower,

subsonic speeds, spanwise flow becomes a problem for swept wings because the incoming flow

has a longer time to react at lower speeds and gets pushed towards the tip, increasing tip stall.

Also, a swept wing decreases aspect ratio which increases induced drag, as shown in Equation 4.

The aspect ratio, along with the other design characteristics of the wing, needs to result in high

lift while minimizing drag, therefore trades and compromises are made to benefit either lift or

drag when necessary.

$$C_{Di} = \frac{C_L^2}{\pi A R e} \qquad \text{Eq. [4]}$$

## 3.3 High-Lift and Control Surfaces

In order to increase lift and achieve shortened takeoff and landing distances, a high-lift

device was incorporated into the design. These devices, such as flaps, slots, and slats, help lift by

increasing the airfoil camber or the wing area. For this light attack aircraft, the type of high-lift

device that was considered was a single-slotted flap. A unique characteristic of this flap is that

there is a gap between the flap and the wing, allowing the airflow to remain attached, which is shown in Figure 10. Many aerodynamic simulations were run on the wings with this flap at different lengths across the span, deflection angles, and widths along the chord. Assuming takeoff conditions, the flap performed the best at a deflection of 50°, a width of 40% up the chord, and a length of 60% across the span.
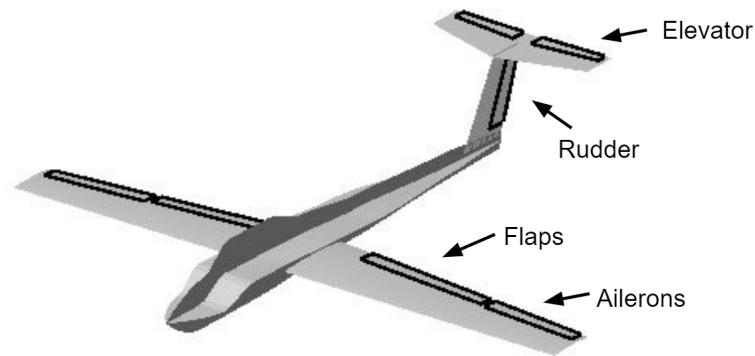


Figure 9: Labeled isometric view of aircraft control surfaces
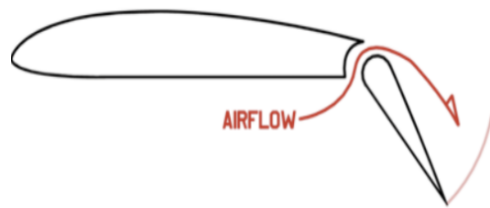


Figure 10: Single-slotted flap depiction

In order to control the aircraft in terms of its roll, pitch, and yaw, other control surfaces had to be implemented on the aircraft to account for them such as ailerons, elevator, and rudder, respectively. The ailerons were placed next to the flaps and took up the rest of the span of the wing and had the same width of the chord as the flaps. With the ailerons pitched at a downward angle of 20°, the moment coefficient about the roll axis was positive and slowly decreased with increasing angle of attack, showing a maximum control of roll at cruise conditions. For the tail,

the elevator control is on the horizontal stabilizer and the yaw control is on the vertical stabilizer,

both of which take up almost the entire span of the stabilizers in order to ensure maximum

control. Also, similar to the ailerons and flaps, they come up about 40% the width of the chord.

With each of those two control surfaces deflected at 20°, the moment coefficients about the pitch

axis and the yaw axis are positive. These results are summarized in Table 5 and all of the control

surfaces are depicted in Figure 9.

Table 5: Moment coefficients for each control surface when deflected at 20° and under cruise
conditions

|  | Roll (x) | Pitch (y) | Yaw (z) |
|---|---|---|---|
| **Moment Coefficient** | 0.11 | 0.75 | 0.097 |

## 3.4 Data Summary

The following table is a summary of the wing design parameters along with some basic

aerodynamic data obtained from VSPaero. The maximum lift coefficient was derived from an

assumed stall angle of 14°. This assumption was based off of the airfoil data charts from

airfoiltools.com that were previously shown in Figure 9 since VSPaero was unable to simulate

flow separation.

Table 6: Summary of Aerodynamic Data

| Parameter | Value |
|---|---|
| Span | 36' |
| Avg c | 4.8' |
| AR | 7.5 (w/ avg c) |
| Taper | 0.5 |
| $C_L$ cruise | 0.5 |
| $C_L$ max | 2.55 w/ flaps |
| $C_{D0}$ cruise | 0.027 |
| $C_{Dtot}$ cruise | 0.032 |
| $C_{Dtot}$ takeoff & landing | 0.2 |

## 4. Propulsion Systems

### 4.1 Propulsion Considerations

The first step to deciding what propulsion system to use on the aircraft was to explore the

pros and cons of several different propulsion systems. The options included turboprop engines,

turbofans, and electric aircraft propulsion. From this, some of the main factors considered in an

engine were T/W ratio, fuel efficiency, flight envelope, and cost. It was found that turbofans

would be too heavy for the aircraft, and in terms of thrust output, they were likely overqualified

for the mission parameters. Next, the current technology in electric aircraft propulsion did not

meet the entry into service of 2025, mainly due to the energy density issues with the batteries

resulting in shorter flight times. With that, it was found that turboprops would suit the mission

requirements as they typically have a suitable weight, enough shaft power to meet the different

segments of the mission, and a lesser unit cost than the other options. Additionally, the turboprop

engine is used in many light attack aircraft. This rationale coupled with the information in Figure

[11] showed that a turboprop engine would be sufficient and optimal.
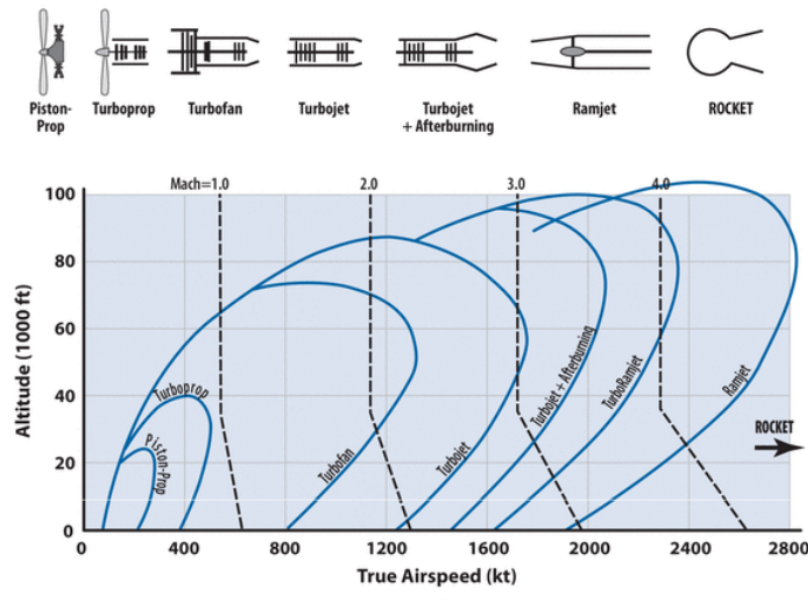


Figure 11: Altitude vs True Airspeed Chart used to determine type of engine

Based on an early estimate using the mission requirements, cruise speed was estimated at

about .4-.5 Mach and 300 kts with a prescribed service ceiling of 30000 feet. Those quantities

along with Figure 11 further confirm that a turboprop engine is suitable for the aircraft.

**4.2 Approach**

From this point, the objective was to decide on an off-the-shelf turboprop engine because

it was a more affordable solution, rather than designing a new, custom engine product with an

anticipated entry into service by 2025. Then, the goal was to recreate that engine's

thermodynamic cycle in GasTurb. GasTurb is a design tool which has several engine schematics

like a turboprop, and easily helps compute gas turbine performance when given input

parameters. Then, once an off-the-shelf engine was selected, research would be performed on

that engine to determine these input parameters into GasTurb. The limitation in this regard is the

information available about the thermodynamic cycle of commercial engines. GasTurb requires

pressure ratios at each station, burner exit temperature, nominal spool speed, several efficiencies,

fuel flow rate, and many other parameters. These are not readily available for many off-the-shelf

engines; however, with thorough research most parameters could be calculated or found.

GasTurb also has a method to model a propeller with specified diameter, RPMs, and

efficiencies. This function will be used in tandem with XROTOR to design the propeller. This

method will yield a complete engine deck with propeller thrust and jet thrust for further mission

analysis. Lastly, several improvements were made to the off-the-shelf engine once it was fully

modeled in GasTurb to account for improvements made to the engine by entry into service.

These changes were supported by further research into improvements in engine efficiency in

recent years.

## 4.3 Engine Selection

The engine selection involved research on different engines as well as informative charts

like Figure 12. Using this figure, trade studies between weight and shaft power are easy to
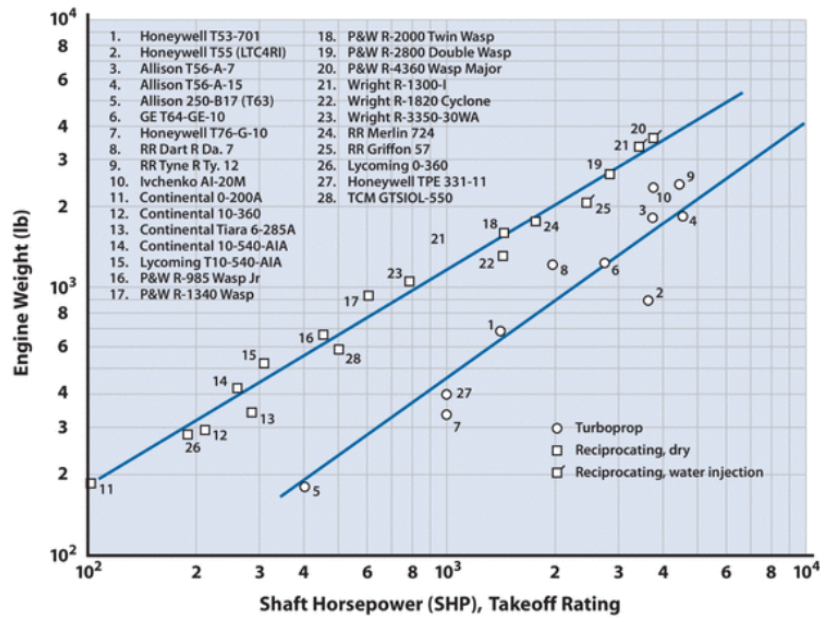
visualize using the bottom line.

Figure 12: Engine Weight vs. Shaft Horsepower (SHP) of various engines from Nicolai and Carichner (2000)

The initial engine selection was heavily informed by the engines on other light attack aircraft. For that engine, we choose a Pratt & Whitney PT6A-65 engine. With the main goal of having a relatively high thrust and low weight, the PT6A-65 has a reported dry weight of 481 with a shaft horsepower of 1249 shp (Pratt & Whitney Canada, 2012). SHP and thrust are related, so the bottom line of Figure 12 can be used to determine if the PT6A-65 performs better in this regard compared to other turboprop engines. When the SHP and weight of the PT6A-65 are plotted on Figure 12, the engine is slightly below the line of best fit, meaning its T/W is slightly better than most of the turboprops shown.

With that, research was done to find the temperature and pressure graph at each stage of the engine shown in Figure 13. From figure 13, the pressure and temperature ratios can be derived and other input parameters were discovered. Moving forward, this engine will be assumed to be more efficient to account for the further development accomplished by the entry into service of 2025.
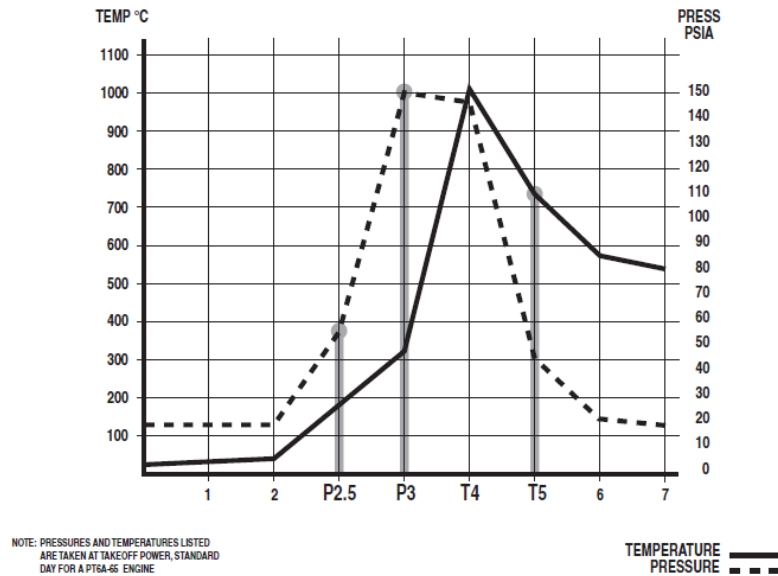
Figure 13: Temperature and Pressure at each stage of PT6A-65

## 4.4 Engine Model and Characteristics

When modeling the PT6A-65, the notable inputs into GasTurb are that a one-spool turboprop was used with several input parameters pictured in Figure 14 with a nominal spool speed of 39,000 rpm and a polytropic turbine efficiency of 0.9.

| Altitude | ft | 0 |
|---|---|---|
| Delta T from ISA | R | 0 |
| Relative Humidity [%] | | 0 |
| Mach Number | | 0 |

| Inlet Corr. Flow W2Rstd | lb/s | 11.0231 |
|---|---|---|
| Intake Pressure Ratio | | 1 |
| Pressure Ratio | | 10.5 |
| Burner Exit Temperature | R | 2291.67 |
| Burner Design Efficiency | | 0.95 |
| Burner Partload Constant | | 1.6 |
| Fuel Heating Value | BTU/lb | 18638 |
| Overboard Bleed | lb/s | 0 |
| Mechanical Efficiency | | 1 |
| Burner Pressure Ratio | | 0.9667 |
| Turbine Exit Duct Press Ratio | | 0.5 |
| Design Exhaust Pressure Ratio | | 1 |

Figure 14: Inputs into GasTurb for base PT6A-65 engine

This engine yielded a net thrust with the propeller of 3282 lb, a TSFC 0.2389 lb/(lb*h), and a SHP of 1200 hp at cruise Mach. Then, this engine was improved to suit an entry into service in 2035, namely by changing three different parameters. First, the overall pressure ratio was changed from 10.5 to 20. This is based on Figure 15, where the year of certification of the PT6A was technically 1960 but it has had improvements since then.



Figure 15: OPR as it changes with year (Avellán, 2011)
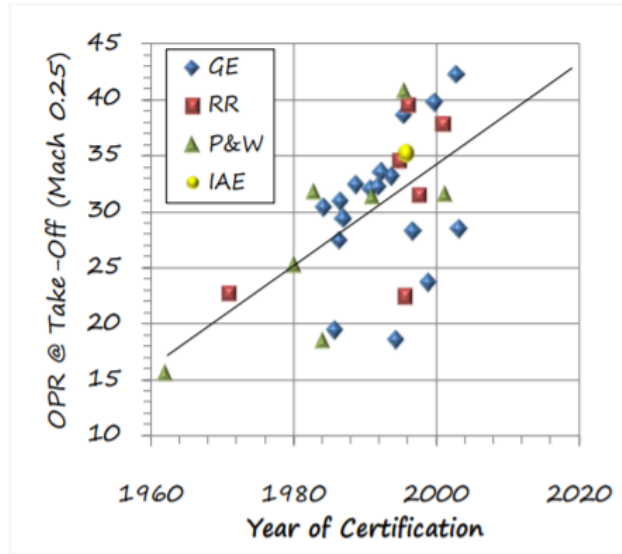
Next, the polytropic efficiency of the turbine was changed based on Figure 16 from .9 to .92, as estimated for the year 2035. Lastly, the turbine exit duct pressure ratio was moved from .5 to .55 because GasTurb flagged that value as low initially. This resulted in a final engine with a thrust of 3646.78 pounds, a TSFC of 0.1778 lb/(lb*h), and 1324.8 hp at cruise Mach.
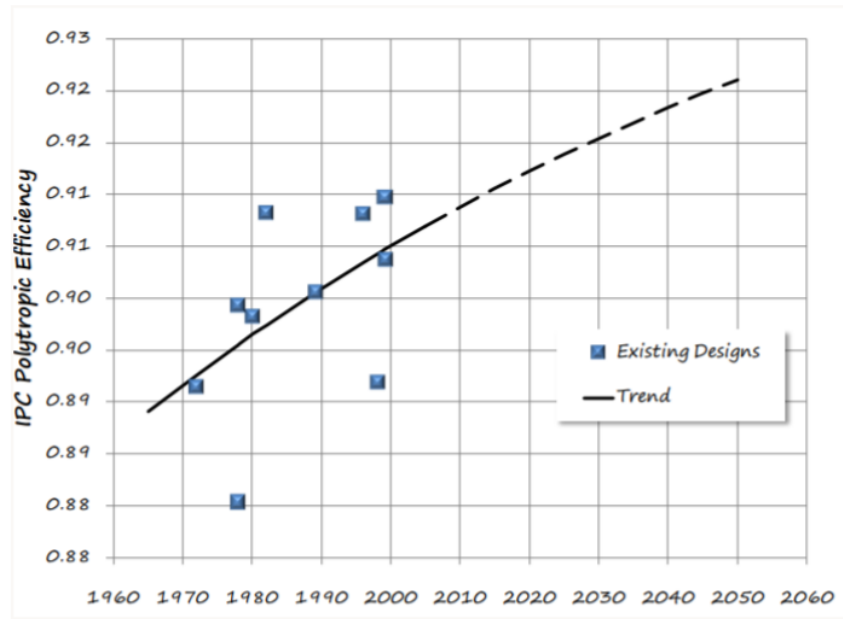
Figure 16: Polytropic Efficiency as a function of year  (Avellán, 2011)

## 4.5 Propeller Model and Characteristics

As seen in the concept downselect table in section 2.1, our team chose a three-bladed, variable pitch propeller design. Using these parameters, plus a diameter of 6.56 feet and an RPM value of 2200, XROTOR produced efficiency values of 0.9039 for prescribed efficiency and 0.8634 for static efficiency. The design was held at a velocity between 145-170 m/s and a power input of 1600 shaft horsepower for each engine. The general value range for diameter, RPM, velocity, and power were chosen based on reference LAA performance and design characteristics, as well as textbook resources for general turboprops. These parameters were then entered into Gasturb to double check between softwares that the thrust being produced for the propeller model was equivalent to the engine model. Many simulations were run between the two softwares to find the appropriate values to ensure our propulsion system would be successful. A lateral and aerial view of the output propeller design is seen in Figure 17.
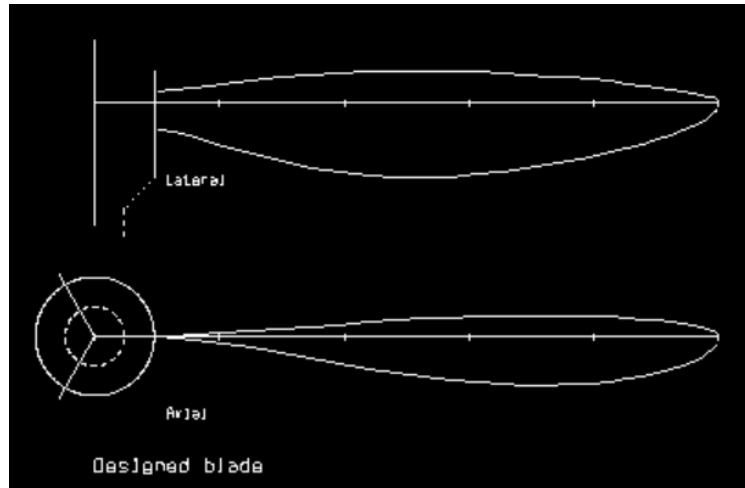
Figure 17: XROTOR propeller design

## 4.6 Engine Sizing

The engine has a length of 75 inches and a diameter of 20 inches. These values are taken from the Pratt & Whitney specifications of the PT6A-65 (Pratt & Whitney Canada, 2012).

## 5. Weight Summary

The center of mass (CM) is located 14 feet from the nose of the LAA when it is fully fueled. As the fuel depletes the CM moves forward about one foot. The calculations for the CM encompassed all of the avionics equipment, pilots, payload configuration and structural weights as seen in Table 7. Figure 18 also shows the CM location graphically, it remains in between the nose and rear landing gear for all of its ranges. Using the FLOPS weight estimation model, the aircraft is estimated to have a TOGW of 16,334 lbs.

## 5.1 Summary Table

Table 7: Summary of all weights

| Component | Percent Weight | Weight (lbs) |
|---|---|---|
| Wing | 7.39 | 1,207 |
| Horizontal Tail | 0.82 | 134 |
| Vertical Tail | 0.63 | 104 |
| Fuselage | 8.58 | 1,402 |
| Landing Gear | 3.68 | 601 |
| Nacelle | 0.73 | 118 |
| **Structures Total** | **21.83** | **3,566** |
| Engines | 5.89 | 962 |
| Miscellaneous Systems | 0.44 | 71 |
| Fuel System-Tanks and Plumbing | 2.82 | 460 |
| **Propulsion Total** | **9.14** | **1,493** |
| Surface Controls | 3.95 | 645 |
| Auxiliary Power | 1.57 | 256 |
| Instruments | 0.76 | 125 |
| Hydraulics | 0.78 | 128 |
| Electrical | 2.60 | 424 |
| Avionics | 1.42 | 232 |
| Furnishings and Equipment | 1.84 | 301 |
| Air Conditioning | 0.52 | 85 |
| **Systems and Equipment Total** | **13.44** | **2,195** |
| **Weight Empty** | **44.42** | **7,255** |
| Crew and Baggage | 2.63 | 430 |

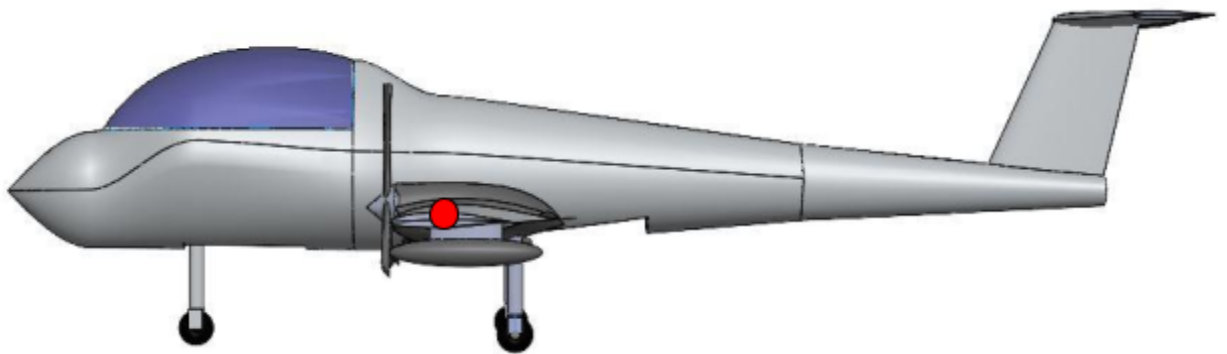| | | |
|---|---:|---:|
| Unusable Fuel | 0.77 | 126 |
| Engine Oil | 0.20 | 33 |
| Miscellaneous | 0.01 | 1 |
| **Operating Weight** | **48.03** | **7,845** |
| Auxiliary Tanks | 0.62 | 101 |
| External Stores | 18.37 | 3,000 |
| **Zero Fuel Weight** | **67.01** | **10,946** |
| Mission Fuel | 32.99 | 5,398 |
| **Ramp (Gross) Weight** | **100.00%** | **16,334** |

Figure 18: Side image depicting the CM

## 5.2 Propulsion

The weight of each engine is 481 lb, making the weight of both engines 962 lb. The total weight for the propulsion system is 1,493 lbs and all of the individual component values can be seen in Table 7 in section 5.

**5.3 Airframe Structure**

The primary component of the airframe for the LAA is the wing structure of the aircraft, seen in Figure 19. Similar to most other aircraft, the LAA's wings use a spar and rib construction for its primary structural support. In order for the spar and ribs to fit into the tapered airfoil, they are also tapered to scale with the airfoil. The spars are a traditional I-beam cross section to maximize moment inertia and increase bending strength while minimizing weight. The ribs are cut to fit the cross section of the wing from root to tip, and each spar is a slightly different geometry due to the different airfoil shapes at the root and tip. Additionally, the spars are hollowed out in the middle to allow for fuel tanks in the wings and to reduce the overall weight of the wing structure. Al 7075-T73510 was selected as the material more the wing structure based on strength requirements of the wing at a maximum design load factor of n=4. The estimated total weight of the wing structure is 1,207 lbs. The total weight of all the components of the airframe structure is estimated to be 3,566 lbs including the wing, tail, fuselage, and nacelle.
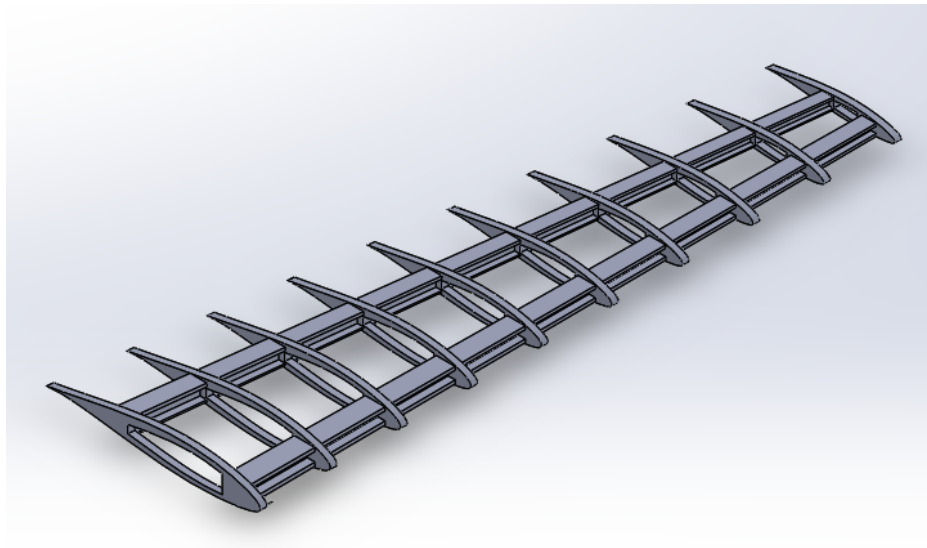


Figure 19: Design for the wing structure

In order to verify the structural integrity of the wing structure within the designed flight envelope, a finite element analysis (FEA) was conducted of the wing structure in Solidworks. In setting up the force distribution, the results from the VSPaero lift distribution analysis were visually analyzed to determine the most accurate model. It was determined that a trapezoidal lift distribution was most appropriate for an accurate analysis, while still maintaining simplicity in the FEA to conserve computational capacity. The lift forces applied to the wing were made to a magnitude such that the maximum design load factor of n=4 was simulated. After generating the mesh, applying constraints, and adding the distributed lift forces to the structure, the FEA model was executed. The results of the FEA model show that the maximum stress in the structure was $3.72*10^6$ Psi, which results in a factor of safety of 1.7 when using the yield strength of the selected material as the limiting parameter. A summary picture of the FEA model of the wing structure is shown below in Figure 20.
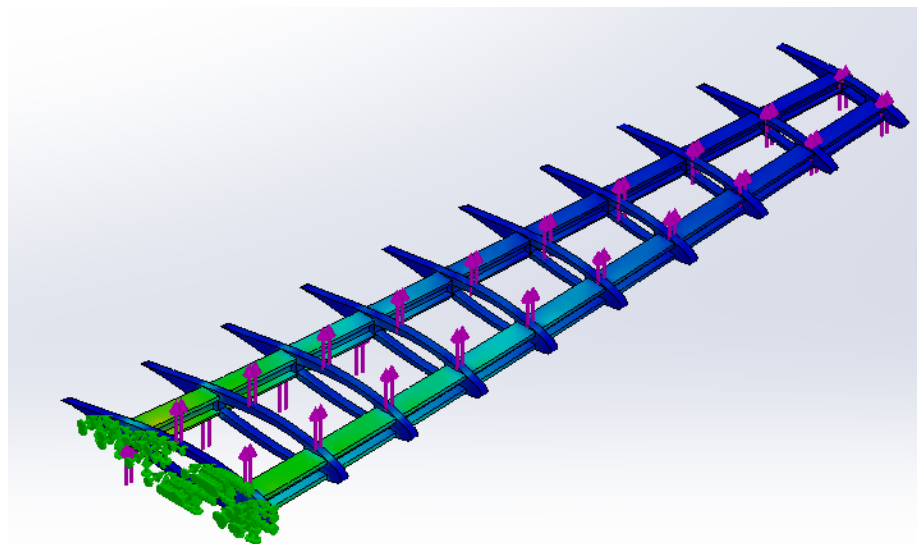


Figure 20: FEA model of the wing structure

**5.4 Crew**

There is room allotted for a crew of two to fit comfortably one in front of the other in the cockpit. There is room for the crew to store water and a few other items which can include food. Each pilot is estimated to be an average of 160 to 230 lbs from the military standards.

**5.5 Payloads**

The RFP requires a minimum of 3000 lbs of armament payload. Our LAA does not have a titanium tub or any additional armament around the fuselage, instead there are chaff and flare countermeasures used to defend against heat seeking missiles. The munitions chosen are as follows, mk 82 bombs, AGM-65 missiles, MAA-1 Infrared bombs, AIM-9 Sidewinder missiles, and Hydra 70 Rocket pods. Not all of these will be attached at one time, instead there are four hard points and an internal bomb bay that allow for adaptive munitions configurations depending on the mission profile. The internal bomb bay was sized to only house two mk 82 bombs, each weighing 500 lbs. In addition to the exterior mounted weapons there are two FN M3P 50 caliber machine guns in the nose of the LAA. Three munitions configurations are possible for the LAA that add up to about 3000 lbs.

*Munitions Configurations*

1. 2 Mk 82 Bombs, 2 AGM-65 Missiles, 2 MAA-1 Infrared Bombs = 2840 lbs

2. 2 Mk 82 Bombs, 2 AGM-65 Missiles, 2 AIM-9 Sidewinder Missiles = 2714 lbs

3. 2 Mk 82 Bombs, 2 AGM-65 Missiles, 2 Hydra 70 Rocket pods = 2834 lbs

Configurations one and three are designed for close air to ground support mainly due to their abundance of bombs and rockets. Configuration three superseides one if the ground targets are greater in numbers and less armored, since the Hydra 70 pods hold up to nineteen rockets.

Two is more of an air-to-air configuration that would not be used often, but the LAA still has the means of equipping it.

**5.6 Fuel/Oil**

The designed LAA has a total usable fuel capacity of 5,470 lbs that is stored in a combination of onboard fuel tanks in the wings and fuselage, as well as in external auxiliary tanks. The estimated oil weight required for the aircraft is 33 lbs, giving a total usable fuel and oil weight of 5,503 lbs.

## 6. Stability and Control

When exploring an aircraft's stability, it is important to recognize the location of the stick-fixed neutral point (aerodynamic center) in reference to the center of gravity. For this aircraft, the aerodynamic center lies about one foot behind the center of gravity, seen in Figure 21, resulting in a positive static margin, meaning that the aircraft will tend to return to its natural state following any perturbation from equilibrium. However, the center of gravity will shift throughout flight due to weight distribution and a reduction in fuel. These shifts require a change in trim force to counteract the movements and maintain stability. For this aircraft, trim is adjusted by minimal adjustments in the control surfaces: ailerons, elevator, and rudder. To further examine the aircraft's stability and control, each control surface axis must be analyzed separately.
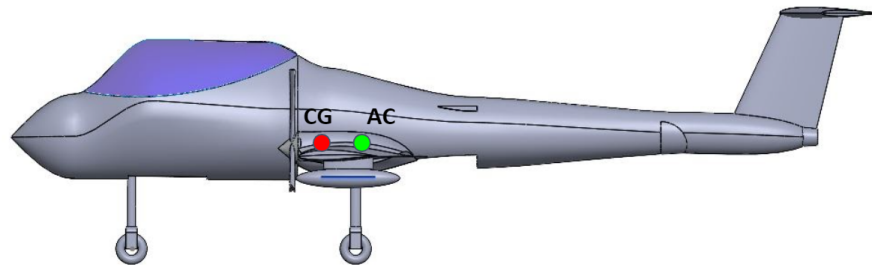
Figure 21: Location of aerodynamic center in reference to the center of gravity

## 6.1 Longitudinal Static Stability

Longitudinal static stability is in reference to the pitching moment. In order to achieve this type of stability, the aircraft's moment coefficient in the pitching plane must be positive at an attack angle of zero, and the change of the moment coefficient with respect to different angles of attack, $C_{M\alpha}$, must be negative. This ensures that the nose of the aircraft will naturally pitch down to equilibrium as the angle of attack increases from natural outside forces like wind. After running an aerodynamic simulation on VSPaero, the results showed that both requirements were satisfied, therefore this aircraft is longitudinally statically stable.

## 6.2 Lateral Static Stability

The lateral motion of the aircraft is the rolling motion about the fuselage centerline. When looking at the front view, the lateral moment is defined as positive with the right wing down below the centerline. Therefore, when perturbed from equilibrium, the change in the moment coefficient with respect to the side slip angle, $C_{\ell\beta}$, must be negative for the right wing to come up for a positive sideslip. An analysis was run on VSPaero that produced a graph showing the lateral moment coefficient decreasing with increasing sideslip angle, therefore the requirement for lateral static stability is satisfied.

**6.3 Directional Static Stability**

The directional motion is the rotation about the vertical yaw axis of the aircraft. Similar to the lateral moment, the directional moment is defined as positive for the right wing down the plane. However, the change in the moment coefficient with respect to the side slip angle, $C_{\eta\beta}$, must be positive to satisfy directional static stability. This ensures that the moments will be generated for a positive sideslip to bring the LAA back towards the centerline. Unfortunately, after running a simulation on VSPaero, the directional moment coefficient was decreasing slightly as the sideslip angle was increasing. Because of the visual observations and symmetry of the aircraft, this could be an error due to the limitations in the VSPaero solver. However, if the lack of directional stability is due to the design of the aircraft, some solutions to this problem include adding a sweep to the wings and moving the vertical tail stabilizer aft. Unfortunately, time constraints did not allow the team to add these design changes, instead these considerations can be used in future work.

## 7. Performance

**7.1 Flight Envelope / V-n Diagram**

To determine the designed flight envelope of the LAA a V-n diagram with gust lines was plotted using equations from Nicolai and Carichner (2000), Miedlar (1997) "User's Guide for FAR23 Loads Program", and Sivakumar Ramakrishnan's (2021) Matlab V-n diagram app. With the V-n diagram and gust lines it is possible to see the limitations of the aircraft and its flight envelope with designed load factors of +4 and -2. The outer set of gust lines are the cruise speed gust lines, and the inner set are the dive speed gust lines. The estimated dive speed for the

designed aircraft is 543 ft/s. The Matlab code for the V-n diagram is located in Appendix B. The

V-n diagram is shown in Figure 22 below.
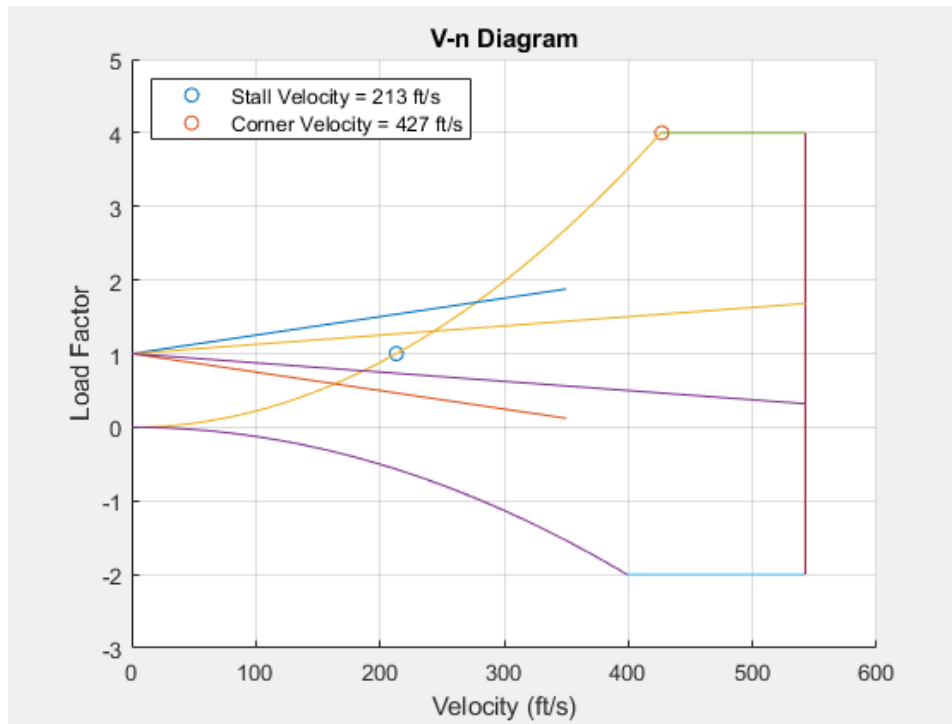


Figure 22: V-n Diagram

In addition to the V-n diagram, a hodograph and power available vs. power required

curves were plotted to get a better understanding of the operational capabilities of the designed

LAA. Both of these plots were calculated using equations and methods that were taught by Dr.

Clayton Geipel and Dr. Meghan Kaminski in their 2020 Flight Vehicle Dynamics course at UVA.

The Matlab code for the hodograph and power curves is available in Appendix C. The hodograph

and power curves are shown in Figures 23 and 24 below.

Figure 23: Hodograph



Figure 24: Power Curve

**7.2 Takeoff and Landing**

According to the RFP, the LAA must be able to take off and land over a 50 ft obstacle on an austere field no longer than 4,000 ft at a density altitude of 6,000 ft. To ensure that this requirement was met, takeoff and landing distance calculations were all conducted at the stated conditions with 100% onboard fuel and payload. The Matlab code for the takeoff and landing distances is available in Appendix D.

*Takeoff*

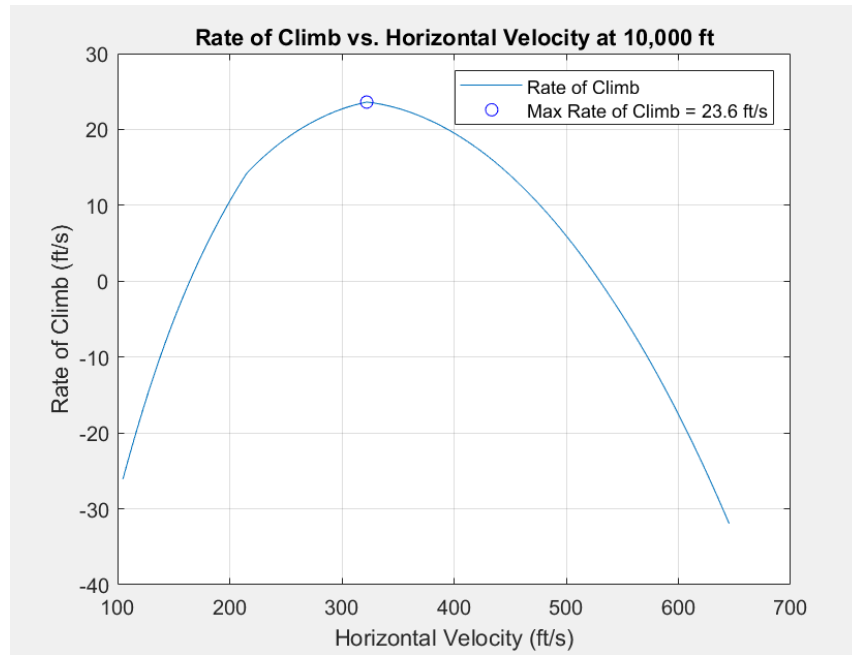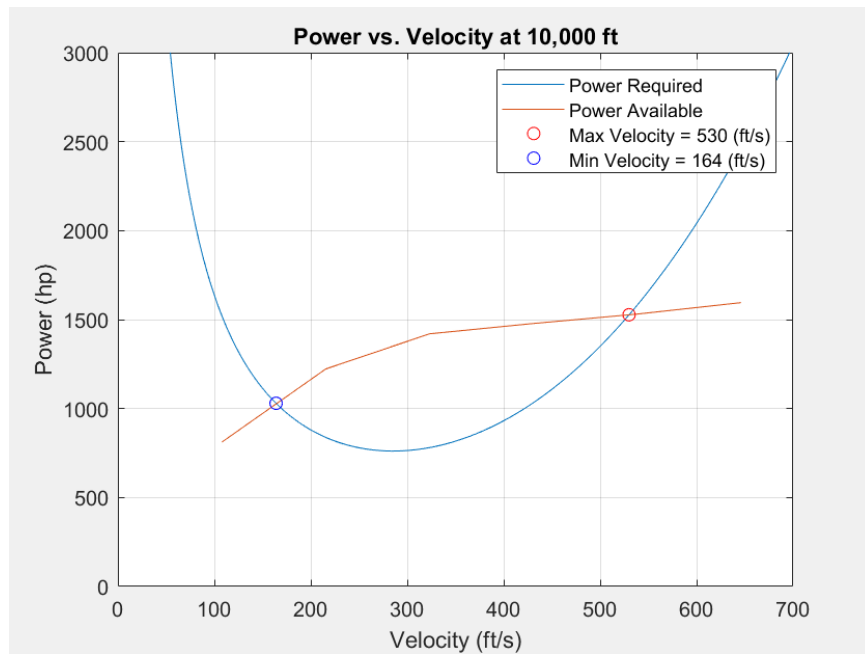The takeoff distance calculation used in the estimation comes from Nicolai and Carichner's (2000) textbook. The takeoff distance was divided into three individual parts: ground distance ($S_G$), rotation distance ($S_R$), and transition distance ($S_{TR}$). Table 8 summarizes the results from the takeoff performance calculations.

Table 8: Takeoff performance calculation results

| Field Type | $S_G$ (ft) | $S_R$ (ft) | $S_{TR}$ (ft) | Total (ft) |
|:---:|:---:|:---:|:---:|:---:|
| Austere | 2,320 | 425 | 966 | 3,711 |

From the above table it can be seen that the LAA meets the maximum takeoff distance requirements for the specified conditions. Under improved takeoff conditions such as less fuel / payload and a lower density altitude the takeoff performance is improved.

*Landing*

The landing distance calculation used in the estimation comes from Nicolai and Carichner's (2000) textbook, just like the takeoff calculation. Similar to the takeoff calculation, the landing calculation was divided into three individual parts: air distance ($S_A$), free roll distance ($S_{FR}$), and braking distance ($S_B$).

Table 9: Landing performance calculation results

| Field Type | $S_A$ (ft) | $S_{FR}$ (ft) | $S_B$ (ft) | Total (ft) |
|:---:|:---:|:---:|:---:|:---:|
| Austere | 1,751 | 666 | 1,168 | 3,585 |

Table 9 shows that the LAA meets the maximum landing distance requirement for the specified conditions. In the calculation of the landing distance reverse thrust was not considered. Under improved landing conditions such as an improved airfield or the usage of reverse thrust the landing distance is improved.

## 7.3 Mission Performance

The aircraft configuration was input into NASA's Flight Optimization System, or FLOPS. Flops is a mission analysis tool that outputs aircraft performance given an aircraft design, and mission profile. The two missions were simulated on FLOPS, and the results are shown below.

*Design Mission*

Table 10: Design Mission Performance

| Mission Segment | Fuel Burned (lbs) | Time (min) | Distance (n mi) |
|:---|---:|---:|---:|
| Taxi and Takeoff | 10 | 5 | 0 |
| Climb | 495 | 18.5 | 85.6 |
| Cruise | 70 | 3.1 | 14.4 |
| Hold | 4104 | 240 | 0 |
| Cruise | 705 | 48.1 | 194.3 |
| Descent | 4 | 1.8 | 7.1 |
| Taxi | 10 | 5 | 0 |
| **Total** | **5,398** | **5.36 hrs** | **301.4** |

As shown in table 10, the aircraft satisfied the RFP requirements for the design mission. In fact, the aircraft was able to cruise on the second segment for 194 n mi, farther than required by the RFP.

*Ferry Mission*

Table 11: Ferry Mission Performance

| Mission Segment | Fuel Burned (lbs) | Time (min) | Distance (n mi) |
|---|---|---|---|
| Taxi and Takeoff | 15 | 5 | 0 |
| Climb | 126 | 8.2 | 16 |
| Cruise | 5,296 | 270.7 | 1396.7 |
| Descent | 4 | 1.2 | 5.4 |
| Taxi | 15 | 5 | 0 |
| **Total** | **5,456** | **4.75 hrs** | **1,418** |

The results shown for the ferry mission in Table 11 also satisfy the RFP. FLOPS ran the simulation with the condition that the cruise segment be flown at the optimum speed and altitude (above 18,000 ft). Again, the aircraft exceeded the required 900 n mi cruise distance by more than 500 n mi.

## 8. Survivability

### 8.1 Austere Field Considerations

Limited ground support means that the more durable and simple replacement components are the better. Our bare-bones approach to the aircraft design means that it can easily be serviced with limited resources and manpower. Stock engine components not only drive down acquisition cost but also means that stock components can be easily sourced around the globe. The landing

gear was designed to be more robust than a standard landing gear setup for aircraft landing on tarmac due to the need to land quickly and in austere fields.

## 8.2 Armaments

For the design mission, the LAA is outfitted with 4 Mk 82 bombs at 500 lb each, as well as 2,000 lbs of various other armaments including .50 caliber machine gun rounds and air to ground missiles. The nose is outfitted with an integrated .50 caliber machine gun for ground targets.

## 8.3 Materials

The main material used will be high strength aluminum due to its strength and lightweight characteristics. The rib structures designed for the wings and fuselage will be aluminum, specifically Al 7075-T73510. Due to the short landing distance requirement and a need for a hard landing, a higher strength material like titanium alloy will be used for the landing gear. The canopy will be multi layered with one layer of polycarbonate, a layer of polyurethane to bond the other two layers, and a layer of polyurethane to bond the other two layers. The total materials cost of the production of all the aircraft was estimated to be $359 Million.

# 9. Cost Analysis & Business Case Analysis

## 9.1 Cost Modeling Approach

To estimate the various cost values associated with the manufacture and distribution of a new aircraft, Advanced Aircraft Analysis (AAA) was used. AAA uses mostly physics based methods alongside some semi empirical methods for its analyses. For cost analysis, however, it is almost all semi empirical methods, using information from previous and existing aircraft as well as an inflation factor to estimate the various costs associated with the aircraft to be analyzed. It is

important to note that AAA is based on data from 1989, but a factor of inflation is included in all calculations.

## 9.2 Acquisition Cost

In order to calculate the total acquisition cost, the engineering and design, program production, and test operations cost must be calculated first to determine key variables that are associated with the total acquisition cost. The engineering and design phase inputs that are associated with the cost that goes into testing the airplane before it is ready for full production. In this case 10 airplanes were manufactured in the research and development phase with a target of 250 airplanes constructed for production in 50 aircraft segments. Using costs associated with airframe and man hours along with the empirical data AAA is equipped with, outputs that are needed for total cost are produced. After this, costs associated with program production are found that are also necessary for calculating the total acquisition cost. After this test operation costs are calculated which factors in the cost associated with test flights after a production airplane is manufactured but before the full production line is manufactured. The total acquisition cost, manufacturing cost, and estimated price per airplane were calculated to be $2.4 billion, $2.15 billion, and $10.6 million, respectively.

Table 12: Price points for Acquisition

| Manufacturer's Profit in Manufacturing Phase | $215.164M |
|---|---|
| Cost to Finance the Manufacturing Phase | $323.746M |
| Total Manufacturing Cost | $2.152B |
| Total Acquisition Cost | $2.367B |
| Estimated Price per Airplane | $10.614M |

## 9.3 Operating Cost

AAA was used to estimate the operating costs as well and required assumptions and inputs from our design. The weight of fuel used was estimated to be 5100 pounds on average for each mission. It was assumed that there would be 1,200 flight hours per year over the 25 year lifespan. It was assumed that once again 250 total aircraft would be produced in 50 aircraft segments. It was assumed that the maintenance crew would make $50,000 a year. Based on research of existing aircraft it was assumed that 22 maintenance man hours would be spent per flight hour. The following table lists the costs found using AAA that are associated with operating costs.

Table 13: Price points for operating

| Program Cost Fuel, Oil, Lubrication | $1.253B |
|---|---|
| Operating Cost per Flight Hour | $2,644 |
| Program Cost Indirect Personnel | $2.593B |
| Maintenance Labor Rate per Hour | $100 |
| Program Cost of Spares | $2.136B |
| Total Operating Cost | $15.258B |

## 9.4 Life Cycle Cost

The Life Cycle Cost on AAA factors in the acquisition, research and development, and operating costs when calculating the Life Cycle Cost. The Life Cycle Cost of the entire program was calculated to be $18 Billion. So for a production run of 250 aircraft this means the Life Cycle Cost of each aircraft is around $72 Million.

## Conclusion

The WB-26 conceptual aircraft was designed to satisfy the requirements and objectives outlined by the RFP. The simplistic design was influenced by a number of existing light attack aircraft, with special attention to making it serviceable on short, unfinished runways in austere environments.

The high lift devices were designed to achieve a takeoff and landing distance less than 4,000 ft over a 50 ft obstacle. The aircraft also leverages the power of two turboprop engines to provide enough thrust to power the takeoff and climb. While the extra weight of the robust power plant system increased the TOGW, the payoff was worth it compared to a single engine configuration.

When carrying out the design and ferry missions, the WB-26 exceeded the requirements outlined by the RFP. Though the actual performance characteristics like rate of climb and speed were not as impressive as perhaps the A-29 or AT-6, the WB-26 was able to complete the missions within the required parameters.

The costs associated with this design seem to match or beat existing aircraft of similar capabilities and mission sets. The operating cost per flight hour as well as the price per aircraft are especially promising numbers. The goal was to design an aircraft that was affordable to purchase and operate and based on the estimations made by AAA, the aircraft exceeds those requirements.

Overall, the WB-26 satisfied the requirements and objectives outlined by the RFP. The final aircraft is conventional by design, which makes it well suited for austere environments where service may be difficult. It dutifully carries out the two mission profiles, while also maintaining a competitive price compared to the industry. Through a number of trade studies, the

aerodynamics and propulsion systems were optimized to suit the requirements. There may be no

perfect plane for these requirements, and while WB-26 is a simple design it harnesses

rudimentary principles for military applications. It gets the job done dutifully and on budget.

## References

AIAA. (2020). Design Competitions - 2021 Undergrad Design RFP. Retrieved October 31, 2020,

from https://www.aiaa.org/get-involved/students-educators/Design-Competitions

Avellán, R. (2011). On the Design of Energy Efficient Aero Engines Some Recent Innovations.

Retrieved April 20, 2021, from

https://publications.lib.chalmers.se/records/fulltext/144502.pdf

AOPA. (2020). AT–6 Wolverine: On the Prowl, the Ultimate Macho Turboprop Single. Retrieved

April 13, 2021, from

https://www.aopa.org/news-and-media/all-news/2020/april/pilot/turbine-at-6-wolverine-o

n-the-prowl

DoD. (2014). *Department of Defense: Airworthiness Certification Criteria* (MIL-HDBK-516C,

Rep.). Wright-Patterson Air Force Base, OH: DoD

DoD. (1998). JSSG-2010 *JOINT SERVICES GUIDE CREW SYSTEMS CRASH PROTECTION*

*HANDBOOK*. http://www.acqnotes.com/Attachments/JSSG-2010-7.pdf

Engler, W. O., Biltgen, P. T., & Mavris, D. N. (2007, January 8). Concept Selection Using an

Interactive Reconfigurable Matrix of Alternatives (IRMA). Retrieved from

https://arc.aiaa.org/doi/10.2514/6.2007-1194.

Geipel, C., & Kaminski, M.  (2020). Propulsion [PowerPoint slides]. Retrieved from University

of Virginia Collab site

Mai, T.. (2017, August 7). *Technology Readiness Level*. NASA. Retrieved October 16, 2020

      from https://techlinkcenter.org/news/technology-readiness-level-dod/

Miedlar P. (1997) *User's Guide for FAR23 Loads Program.*

      http://www.tc.faa.gov/its/worldpac/techrpt/ar96-46.pdf

Nicolai, L. M., & Carichner, G. (2000). *Fundamentals of aircraft and airship design*. ProQuest

      Ebook Central https://ebookcentral-proquest-com.proxy01.its.virginia.edu

OpenVSP (Version 3.23.0) [Computer software]. (2021). Retrieved from http://openvsp.org/

Pratt & Whitney Canada (2012). *Design Specifications Sheet for PT6-A Variants.*

Ramakrishnan, S. (2021). V-n Diagram [Computer Program]. Retrieved from

      https://www.mathworks.com/matlabcentral/fileexchange/81793-v-n-diagram

Sierra Nevada Corporation. (2018, July 18). A-29 Specifications - A-29 for America: Super

      Tucano: OA-X. Retrieved April 13 2021, from

      https://www.builtforthemission.com/a-29-super-tucano/a-29-specs/

## Appendices

Appendix A:

```
%Wade Boggs TOGW Initial Estimation
clear
clc

TOGW_m = [];
w_e_a_m = [];
n_m = [];
for n = 303800:6076:3038000
    n_m = [n_m, n];
    TOGW = 15000; %Initial Guess
    c = weight_fuel_frac(n); %Fuel weight constant
    w_f = TOGW*c; %Initial fuel weight guess
    w_fixed = 4329.6; %Fixed Weight
    w_e_g = TOGW - w_f - w_fixed; %Initially guessed empty weight
    w_e_a = 0.774*TOGW^(0.947); %Empty weight according to the equation
    while abs(w_e_g - w_e_a) > 0.01*w_e_a %Iterating until the guessed empty weight agrees
with the empty weight predicted from the equation
        if w_e_g - w_e_a < 0
            TOGW = TOGW +1;
        else
            TOGW = TOGW -1;
        end
        w_f = TOGW*c; %Recalculating fuel weight
        w_e_g = TOGW - w_f - w_fixed; %Recalculating guessed empty weight
        w_e_a = 0.774*TOGW^(0.947);  %Recalculating equation estimated
    end
    TOGW_m = [TOGW_m, TOGW];
    w_e_a_m = [w_e_a_m, w_e_a];
end
plot(n_m./6076,TOGW_m)
TOGW_m(100)
W_fuel = TOGW_m(100)*weight_fuel_frac(100*6076);
w_e_a_m(100);
%x = 1e4:2:1e5;
%y = 0.911*x.^(0.947);
%loglog(x,y);
```

```
%hold on;
%plot(TOGW,w_e_a,'r*');
%xlabel('Takeoff Gross Weight (lb)');
%ylabel('Empty Weight (lb)');
%legend('Empty Weight vs. Gross Weight','Convergence Point W_e = 11091 lb, TOGW = 20611 lb');
%title('Empty Weight vs. Takeoff Gross Weight','W_e = 0.911*TOGW*pwr(0.947)');
%weight of fuel estimate
%%%%%%%%%%%%%%%%%%%%%%%%%%%%%%%%%%%%%%%%%%%%%%%%%%%%%%%%%%%%%
%%%%%%%%%%%%%%%%%%%%%%%%%%%%%%%%%%%%%%%%
%variables
R = 100*6076.11549; %range for first and second cruise (phase 4 and 8) in feet
R_ferry = 900*6076.11549; %range for ferry cruise
TSFC = .34/3600; %from Appendix J in book, converted to lb/s/lb
C_d0 = .022; %table
AR = 8.5; %from AT-6 or A-29 AR
e = .9; %oswald efficiency, idk this is what it normally is
K = 1/(pi*AR*e);
L_D = 1/(2*sqrt(C_d0*K));
M = .6; %assumed to be .6 at cruise as it is before the transonic drag rise
gamma = 1.4; %ratio of specific heats for air
gas_R = 1716; %gas constant for air in J/(kg*K)
T_10000 = 482.97; %in Rankine
T_18000 = 454.47; %in Rankine
T_30000 = 411.84; %in Rankine
V_cruise = M*sqrt(gamma*gas_R*T_10000);
V_cruise_30000 = M*sqrt(gamma*gas_R*T_30000);
V_cruise_18000 = M*sqrt(gamma*gas_R*T_18000);
E = 4*3600; %endurance for loiter (stage 6) in seconds
E_reserve = .75*3600; %endurance for loiter during reserves

%Design mission with cruise altitude at 10000 feet
W_2_1 = .995; %warm-up/taxi, assumed from empirical data
W_3_2 = .97; %take off, about 3% fuel .97 burn assumed from empirical data
W_4_3 = .98; %climb, from fig 5.2 w/ Mach number approx = .6
W_5_4 = exp(-(R*TSFC)/(V_cruise*(L_D))); %cruise
W_6_5 = .97; %relative to known Descent/Landing values
W_7_6 = exp(-(E*TSFC)/(L_D)); %loiter
W_8_7 = W_4_3; %same as climb as well
W_9_8 = W_5_4; %same as cruise, assumed at same altitude
```

W_10_9 = .975; %assumed from empirical data
W_11_10 = .995; %assumed from empirical data
W_12_11 = .98; %assumed from empirical data
W_13_12 = exp(-(E_reserve*TSFC)/(L_D)); %loiter reserve phase

W_13_1 =
W_2_1*W_3_2*W_4_3*W_5_4*W_6_5*W_7_6*W_8_7*W_9_8*W_10_9*W_11_10*W_12_
11*W_13_12;

W_trapped_TO = .01; %assumed from empirical data
W_fuel_design_10000 = (1 + W_trapped_TO)*(1 - W_13_1);

%Ferry mission at 18000 ft
W_2_1 = .995; %warm-up/taxi, assumed from empirical data
W_3_2 = .97; %take off, about 3% fuel .97 burn assumed from empirical data
W_4_3 = .98; %climb, from figure 5.2 w/ MAch = .6
W_5_4 = exp(-(R_ferry*TSFC)/(V_cruise_18000*(L_D))); %cruise at 18000 feet
W_6_5 = .975; %descent/landing, from empirical data
W_7_6 = .995; %taxi/shutdown, form empirical data
W_8_7 = .98; %reserves for climb, from fig 5.2
W_9_8 = exp(-(E_reserve*TSFC)/(L_D)); %loiter reserve phase

W_9_1 = W_2_1*W_3_2*W_4_3*W_5_4*W_6_5*W_7_6*W_8_7*W_9_8;
W_fuel_ferry_18000 = (1 + W_trapped_TO)*(1 - W_9_1);

%Ferry mission at 30000 ft
W_2_1 = .995; %warm-up/taxi, assumed from empirical data
W_3_2 = .97; %take off, about 3% fuel .97 burn assumed from empirical data
W_4_3 = .98; %climb, from figure 5.2 w/ MAch = .6
W_5_4 = exp(-(R_ferry*TSFC)/(V_cruise_30000*(L_D))); %cruise at 18000 feet
W_6_5 = .975; %descent/landing, from empirical data
W_7_6 = .995; %taxi/shutdown, form empirical data
W_8_7 = .98; %reserves for climb, from fig 5.2
W_9_8 = exp(-(E_reserve*TSFC)/(L_D)); %loiter reserve phase

W_9_1 = W_2_1*W_3_2*W_4_3*W_5_4*W_6_5*W_7_6*W_8_7*W_9_8;
W_fuel_ferry_30000 = (1 + W_trapped_TO)*(1 - W_9_1);


function W_fuel_design_30000 = weight_fuel_frac(r)

```
TSFC = .34/3600; %from Appendix J in book, converted to lb/s/lb
C_d0 = .020; %table
AR = 6.4; %from AT-6 or A-29 AR
e = .9; %oswald efficiency, idk this is what it normally is
K = 1/(pi*AR*e);
L_D = 1/(2*sqrt(C_d0*K));
M = .5; %assumed to be .6 at cruise as it is before the transonic drag rise
gamma = 1.4; %ratio of specific heats for air
gas_R = 1716; %gas constant for air in J/(kg*K)
T_30000 = 411.84; %in Rankine
V_cruise_30000 = M*sqrt(gamma*gas_R*T_30000);
E = 4*3600; %endurance for loiter (stage 6) in seconds
E_reserve = .75*3600; %endurance for loiter during reserves
%Design mission- If cruise was at service ceiling, altitude equal to 30000 ft
W_2_1 = .995; %warm-up/taxi, assumed from empirical data
W_3_2 = .97; %take off, about 3% fuel .97 burn assumed from empirical data
W_4_3 = .98; %climb, from fig 5.2 w/ Mach number approx = .6
W_5_4 = exp(-(r*TSFC)/(V_cruise_30000*(L_D))); %cruise at 30000 feet
W_6_5 = .97; %relative to known Descent/Landing values
W_7_6 = exp(-(E*TSFC)/(L_D)); %loiter
W_8_7 = W_4_3; %same as climb as well
W_9_8 = W_5_4; %same as cruise, assumed at same altitude
W_10_9 = .975; %descent/landing, assumed from empirical data
W_11_10 = .995; %taxi/shutdown, assumed from empirical data
W_12_11 = .98; %reserves for climb, from fig 5.2
W_13_12 = exp(-(E_reserve*TSFC)/(L_D)); %loiter reserve phase

    W_13_1 =
W_2_1*W_3_2*W_4_3*W_5_4*W_6_5*W_7_6*W_8_7*W_9_8*W_10_9*W_11_10*W_12_
11*W_13_12;

    W_trapped_TO = .01; %assumed from empirical data

    W_fuel_design_30000 = (1 + W_trapped_TO)*(1 - W_13_1);
end
```

Appendix B:

```
%Wade Boggs V-n Diagram
s = 172.8;
Cl_max = 1.75;
Cl_min = 1;
rho = .002378;
W = 15049;
n_max = 4;
n_min = -2;
v_stall_1 = ((2*W)/(rho*s*Cl_max))^(.5);
v_a = ceil(v_stall_1*(n_max)^(.5));
v_1 = 0:1:v_a;
v_stall_2 = ((2*W)/(rho*s*Cl_min))^(.5);
v_g = ceil(v_stall_2*(abs(n_min))^(.5));
v_2 = 0:1:v_g;
n_aero_max = ((.5)*rho*s*Cl_max*v_1.^2)/(W);
n_aero_min = -((.5)*rho*s*Cl_min*v_2.^2)/(W);
v_c = 33*(W/s)^(.5);
v_d = 1.55*v_c;
v_3 = v_a:1:v_d;
v_4 = v_g:1:v_d;
n_3 = n_max*ones(1,length(v_3));
n_4 = n_min*ones(1,length(v_4));
n_5 = n_min:.1:n_max;
v_5 = v_d*ones(1,length(n_5));
index_stall = find(v_1 == round(v_stall_1));
scatter(v_stall_1,n_aero_max(index_stall));
hold on
scatter(max(v_1),n_max);
hold on
plot(v_1,n_aero_max);
hold on
plot (v_2,n_aero_min);
hold on
plot(v_3,n_3);
hold on
plot(v_4,n_4);
hold on
plot(v_5,n_5);
```

```
title('V-n Diagram');
xlabel('Velocity (ft/s)');
ylabel('Load Factor');
grid
index_stall = find(v_1 == round(v_stall_1));
legend({'Stall Velocity = 205 ft/s','Corner Velocity = 410 ft/s'},'location','northwest')
```

Appendix C: Aircraft Hodograph and Power Curves Matlab Code

```
%Wade Boggs Aircraft Performance
v1=108:1:215;
v2=216:1:323;
v3=324:1:431;
v4=432:1:539;
v5=540:1:646;
pa1=3.817.*v1+399.96;
pa2=1.8355.*v2+826.99;
pa3=0.5388.*v3+1246;
pa4=0.491.*v4+1266.6;
pa5=0.5975.*v5+1209.3;
pa=[pa1 pa2 pa3 pa4 pa5];
va=[v1 v2 v3 v4 v5];
P=17.56*10^(-4);
s=172.8;
cd=.03;
e=0.7;
AR=7.5;
v=1:1:750;
q=(.5*P*v.^2);
w=15049;
cl=w./(q*s);
tr=q.*s.*(cd+((cl.^2)/(pi*e*AR)));
pr=.0018.*tr.*v;
diff = [];
diff_i = [];
for i = 1:length(v4);
    d=abs(pr(i+431)-pa4(i));
    diff = [diff d];
end
```

```
for i = 1:length(v1);
    g=abs(pr(i+107)-pa1(i));
    diff_i = [diff_i g];
end
[difference,index] = min(diff);
[difference_i,index_i] = min(diff_i);
max_vel = v(index+431)
min_vel = v(index_i+107)
roc=[];
vh=[];
for i=1:length(pa);
    j = (pa(i)-pr(i+107))/(w*.0018);
    z = ((va(i))^(2)-j^(2))^(.5);
    roc=[roc j];
    vh=[vh z];
end
[max_roc,max_roc_index]=max(roc)
figure(1)
plot(v,pr);
hold on
plot(va,pa);
ylim([0 3000])
title('Power vs. Velocity at 10,000 ft');
xlabel('Velocity (ft/s)');
ylabel('Power (hp)');
scatter(max_vel,pr(index+431),'red')
scatter(min_vel,pr(index_i+107),'blue')
legend({'Power Required','Power Available','Max Velocity = 530 (ft/s)','Min Velocity = 164
(ft/s)'},'Location','northeast');
grid on
hold off
figure(2)
plot(vh,roc);
title('Rate of Climb vs. Horizontal Velocity at 10,000 ft');
xlabel('Horizontal Velocity (ft/s)');
ylabel('Rate of Climb (ft/s)');
grid on
hold on
scatter(vh(max_roc_index),max_roc,'blue');
legend({'Rate of Climb','Max Rate of Climb = 23.6 ft/s'},'Location','northeast');
```

Appendix D: Takeoff and Landing Distance Matlab Code

```matlab
%Wade Boggs Takeoff and Landing Distance
W_to = 16334; %lbs;
S_ref = 172.8; %ft^2;
rho = 19.87*10^(-4); %slug/ft^3
c_lmax = 2.55;
v_stall = ((W_to*2)/(S_ref*rho*c_lmax))^(.5); %ft/s
v_to = 1.1*v_stall;
v_avg = 0.707*v_to; %ft/s
g = 32.2; %ft/s^2
c_d = 0.032;
c_dg = 0.0125;
c_lg = 0.5;
mu = .015;
T_to = 6262.2;
D_to = (.5)*(rho*(v_avg^2)*S_ref)*(c_d+c_dg); %lb
L_to = (.5)*(rho*(v_avg^2)*S_ref)*c_lg; %lb
S_g = (1.44*(W_to/S_ref))/(g*rho*c_lmax*((T_to/W_to)-(D_to/W_to)-mu*(1-(L_to/W_to))));
%ft
S_r = 2*v_to; % ft
R = (v_to^2)/(0.15*g);
theta = acos((R-50)/R);
S_tr = R*sin(theta);
S_to_tot = S_g + S_r + S_tr
v_app = 1.3*v_stall;
v_td = 1.15*v_stall;
W_f = 3835; %lbs
W_l = W_to - 0.5*W_f; %lbs
c_dl = 0.2;
mu_b = 0.6;
D_l = 0.5*rho*((v_app)^2)*S_ref*(c_dl);
S_a = (W_l/D_l)*(((v_app^2)-(v_td^2))/(2*g) + 50);
S_fr = 3*v_td;
S_b = (W_l/(g*mu_b*rho*S_ref*(((c_dl)/mu_b) - c_lg)))*log(1+((rho*S_ref)/(2*W_l))*(((c_dl
+ c_dg)/mu_b)-c_lg)*(v_td^2));
S_ld_tot = S_a + S_fr + S_b
```